

**Discrete Superconducting Phases in FeSe-Derived Superconductors**

T. P. Ying,<sup>1</sup> M. X. Wang,<sup>1</sup> X. X. Wu,<sup>2</sup> Z. Y. Zhao,<sup>1</sup> Z. Z. Zhang,<sup>3</sup> B. Q. Song,<sup>1</sup> Y. C. Li,<sup>1</sup> B. Lei,<sup>4</sup>  
 Q. Li,<sup>1</sup> Y. Yu,<sup>1</sup> E. J. Cheng,<sup>1</sup> Z. H. An,<sup>1</sup> Y. Zhang,<sup>1,5</sup> X. Y. Jia,<sup>1</sup> W. Yang,<sup>6</sup>  
 X. H. Chen,<sup>4,5,\*</sup> and S. Y. Li<sup>1,5,†</sup>

<sup>1</sup>*State Key Laboratory of Surface Physics, Department of Physics, and Laboratory of Advanced Materials, Fudan University, Shanghai 200438, China*

<sup>2</sup>*Institut für Theoretische Physik und Astrophysik, Julius-Maximilians-Universität Würzburg, 97074 Würzburg, Germany*

<sup>3</sup>*Key Laboratory for Renewable Energy, Beijing Key Laboratory for New Energy Materials and Devices, Beijing National Laboratory for Condensed Matter Physics, Institute of Physics, Chinese Academy of Sciences, School of Physical Sciences, University of Chinese Academy of Sciences, Beijing 100190, China*

<sup>4</sup>*Hefei National Laboratory for Physical Sciences at Microscale and Department of Physics, and Key Laboratory of Strongly-Coupled Quantum Matter Physics, Chinese Academy of Sciences, University of Science and Technology of China, Hefei, Anhui 230026, China*

<sup>5</sup>*Collaborative Innovation Center of Advanced Microstructures, Nanjing 210093, China*

<sup>6</sup>*Tianmu Lake Institute of Advanced Energy Storage Technologies, Liyang, Jiangsu 213300, China*



(Received 13 March 2018; published 15 November 2018)

A general feature of unconventional superconductors is the existence of a superconducting dome in the phase diagram. Here we report a series of discrete superconducting phases in the simplest iron-based superconductor, FeSe thin flakes, by continuously tuning the carrier concentration through the intercalation of Li and Na ions with a solid ionic gating technique. Such discrete superconducting phases are robust against the substitution of 20% S for Se, but they are vulnerable to the substitution of 2% Cu for Fe, highlighting the importance of the iron site being intact. The superconducting phase diagram for FeSe derivatives is given, which is distinct from that of other unconventional superconductors.

DOI: [10.1103/PhysRevLett.121.207003](https://doi.org/10.1103/PhysRevLett.121.207003)

The discovery of iron-based superconductors sparked a huge renaissance in exploring the mystery of unconventional superconductivity [1,2]. For the iron arsenides, there always exists a superconducting (SC) dome in the phase diagram, i.e., a continuous increase, maximum, and then decrease of the transition temperature  $T_c$ , with charge carrier doping, applied external pressure, or isovalent doping [3–6]. Such a SC dome is a common feature shared by other unconventional superconductors, such as cuprate, heavy-fermion, and organic superconductors [7].

Iron selenide has recently attracted great interest, since its  $T_c$  (= 8 K) can be significantly enhanced by electron doping and external pressure [8–13], even up to 65 K in monolayer FeSe/SrTiO<sub>3</sub>, possibly with the assistance of phonons from the substrate [14–17]. A robust  $T_c$  of ~32 K was first discovered in K<sub>x</sub>Fe<sub>2–y</sub>Se<sub>2</sub>, followed by an occasional observation of trace superconductivity at 44 K [4,5]. However, attempts to build a phase diagram have been hampered by the prevalence of phase separation which arises inevitably from the high-temperature synthesis routes [3–6]. An alternative strategy to obtain single-phase samples and avoid phase separation is to use a low-temperature solvent such as liquid ammonia or to employ the electrochemical technique, but

drawbacks include limited control over the intercalation of metals and sample inhomogeneity [4–6,18,19].

The electrostatic gating technique provides precise control of the doping content and consequently the physical properties of a material [20]. In previous electrostatic gating of FeSe flakes, using ionic liquid as the gate dielectric, a rise in  $T_c$  was reported at a certain gate voltage due to a Lifshitz transition, followed by a gradual increase of  $T_c$  from ~30 to 48 K [21]. Insulating FeSe thin films were successfully converted into superconductors with  $T_c$  increasing to about 40 K [22,23]. However, the charge accumulation induced by liquid ionic gating is confined to the very subsurface due to the Thomas-Fermi screening effect [24], and the doping level is limited due to sample damage at high gate voltages [21–23].

In this Letter, by using the latest developed solid ionic gating technique [25], we continuously intercalate Li/Na into FeSe flakes and construct the entire phase diagram of metal-intercalated FeSe superconductors. Starting from the  $T_c = 8$  K phase, two subsequent SC phases with  $T_c$ 's of ~36 and ~44 K are observed upon increasing the intercalation of Li, and finally the system enters an insulating state. Similar discrete SC phases are also found in Na<sub>x</sub>FeSe.

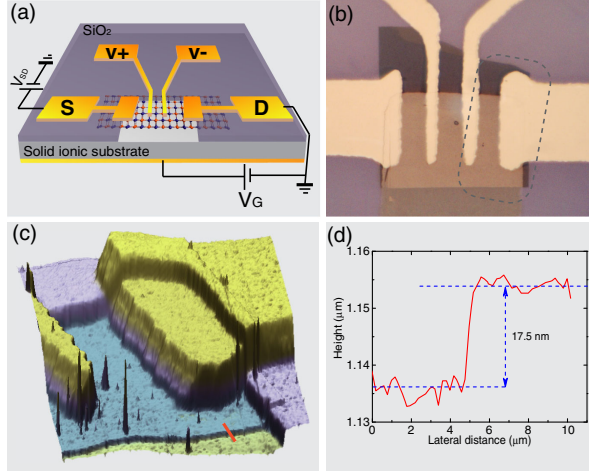


FIG. 1. (a) Schematic structure of the solid ionic gating device. From the bottom to the top: Silver back gate layer, finely polished Li/Na-ion substrate, pure or doped FeSe thin flake, 100 nm  $\text{SiO}_2$ , and four electrodes. The gate voltage  $V_G$  is applied at low temperature ( $<155$  K), where all the ions in the substrate are frozen in place. (b) Representative optical image of a fabricated device. Shadow masks are used here to eliminate any contamination from the photoresist or developer. (c) Atomic force microscope (AFM) topographic image of the dashed rectangular area shown in (b). (d) Cross-sectional profile of the thin flake along the red line in (c), giving the thickness of the flake  $t = 17.5$  nm, which corresponds to about 31 FeSe monolayers. The thickness of the samples used in the present study ranges from 5 to 38 nm.

Considering the continuity of Li/Na intercalation, such discrete SC phases must be intrinsic and universal for FeSe derivatives obtained by metal intercalation. We find that these discrete SC phases are easily destroyed by a small amount of copper substitution at the iron site, but they are insensitive to sulfur substitution at the selenium site. A comprehensive phase diagram of FeSe-derived superconductors is obtained in combination with previous surface spectroscopic studies.

FeSe,  $\text{FeSe}_{0.80(1)}\text{S}_{0.20(1)}$ ,  $\text{Fe}_{0.98(1)}\text{Cu}_{0.02(1)}\text{Se}$ , and  $\text{Fe}_{0.95(1)}\text{Cu}_{0.04(1)}\text{Se}$  were mechanically exfoliated by Scotch Tape and transferred to lithium-based substrate  $\text{Li}_{1+x+y}\text{Al}_x(\text{Ti, Ge})_{2-x}\text{Si}_y\text{P}_{3-y}\text{O}_{12}$  and sodium-based substrate  $\text{Na}_{3.4}\text{Zr}_{1.8}\text{Mg}_{0.2}\text{Si}_2\text{PO}_{12}$  [26]. Transport measurements were carried out in a physical properties measurement system (PPMS, Quantum Design) equipped with a Keithley 2400 source meter (with rms noise about 20 pA) to apply the gate voltage, and a lock-in amplifier (SR830) to measure its resistance. Density functional theory (DFT) calculations employed the projector augmented wave (PAW) method encoded in the Vienna *ab initio* simulation package (VASP). Detailed descriptions can be found in the Supplemental Material [27].

Figure 1(a) shows the configuration of the fabricated solid ionic gating device. A single FeSe thin flake with a thickness of 5–38 nm (9–68 monolayers) is sandwiched

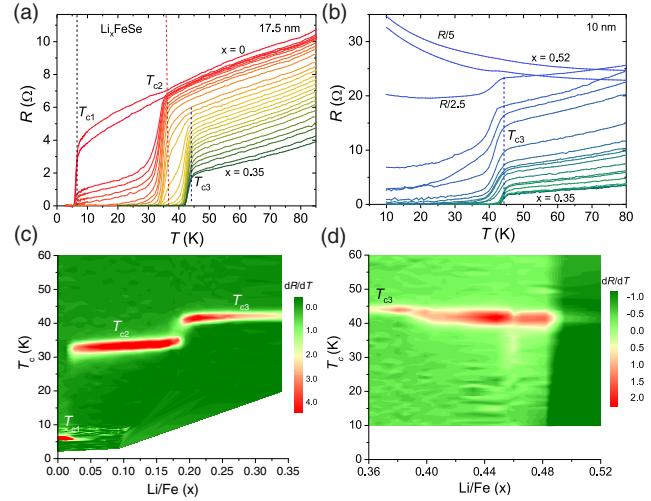


FIG. 2. (a) Resistance of the Li-intercalated FeSe flake (17.5 nm) as a function of temperature. This panel covers the underdoped regime with the normal-state resistance monotonically decreasing upon gating. Colored dashed lines highlight transition temperatures where the  $T_c$ 's (in this work, we use  $T_c^{\text{onset}}$  as  $T_c$ ) of several curves coincide.  $T_{c1}$ ,  $T_{c2}$ , and  $T_{c3}$  are SC phases at 8, 36, and 44 K, respectively. (b) Resistance of another 10 nm FeSe flake in the overdoped regime with its normal-state resistance gradually increasing upon gating. (c) and (d) Color contour plots of the derivatives of the  $R - T$  curves in (a) and (b). We rescaled the curves in (b) at 80 K before differentiating to see the SC transitions more clearly.

between the solid ionic substrate and a  $\text{SiO}_2$  layer, as shown in Figs. 1(b) and 1(c). We use 100 nm  $\text{SiO}_2$  to insulate the electrodes from the substrate to avoid metal accumulation underneath the electrodes. This insulating layer is crucial to accurately determining the content of the intercalated metals. A window is left open on the  $\text{SiO}_2$  layer to pattern the silver electrodes. When a back gate voltage,  $V_G = 4$  V, is applied at low temperature (usually below 155 K), all the lithium or sodium ions in the substrate are still frozen in place. Upon slowly heating the device above 165 K, these ions become mobile and are driven into the sample by the electric field. The ionic mobility is monitored by the leakage current; see Fig. S1 in the Supplemental Material [27].

We first examine the lightly doped region of  $\text{Li}_x\text{FeSe}$ . By carefully choosing the gating temperature and integrating leakage current, the lithium content  $x$  can be tuned with a precision of 1% (see the Supplemental Material [27]). A single FeSe flake with a thickness of 17.5 nm [31 monolayers, shown in Fig. 1(d)] is used, and the resistance as a function of temperature upon gating is plotted in Fig. 2(a). Strikingly, a SC transition with  $T_{c2} \approx 36$  K appears abruptly with negligible changes in the normal-state resistance, coexisting with the SC transition at  $T_{c1} = 8$  K (the bulk  $T_c$  of FeSe). The transition at 8 K is then quickly suppressed, and the normal-state resistance continuously decreases upon increasing the doping level by the intercalation of Li. Meanwhile, the new SC transition remains at 36 K, but it

becomes sharper and sharper. Upon further increasing the Li content, another SC transition at  $T_{c3} = 44$  K sets in, coexisting with the 36 K phase. The 36 K SC phase is then suppressed until only the 44 K SC phase remains. As shown in Fig. 2(b), the normal-state resistance increases upon further gating, and the SC phase at 44 K gradually disappears until the sample eventually enters an insulating phase. The observation of an insulating phase gives a strong evidence of bulk intercalation, since the dopants must diffuse all the way across the sample to the electrodes. Otherwise, the surviving SC phase on that side of the sample would short-circuit the electrodes. Since the gating process is very time consuming, the results shown in Fig. 2(b) are obtained for another 10-nm-thick sample.

To distinguish these SC phases, we compute the derivatives  $dR/dT$  of each  $R - T$  curve and plot the results as color contours in Figs. 2(c) and 2(d). The Li/Fe-ratio dependence of  $T_c$  shows steplike behavior throughout the entire accessible doping range. The  $T_{c2}$  phase emerges at a very low doping content ( $x \approx 0.025$ ), and it is replaced by the 44 K phase at  $x \approx 0.17$ . These results demonstrate that the SC phases in  $\text{Li}_x\text{FeSe}$  are discrete rather than a continuous dome as observed in iron arsenides and other unconventional superconductors.

The previously reported 44 K phase was acquired by lithium intercalation with the assistance of organic molecules such as  $\text{NH}_3$  [10,11,35]. The Li content in  $\text{Li}_{0.6(1)}(\text{ND}_2)_{0.2(1)}(\text{ND}_3)_{0.8(1)}\text{Fe}_2\text{Se}_2$  was determined by refining the neutron powder diffraction pattern [35]. To determine whether our  $T_{c3} = 44$  K phase is the same SC phase observed previously, we need to compare the Li content in them. During the gating process, the observation of two SC transitions suggests the coexistence of two SC phases. Once the SC transition at  $T_{c1} = 8$  K disappears, the SC transition at  $T_{c2} = 36$  K becomes sharper upon further gating. We assume that only one single SC phase exists in the system when the transition at 36 K is sharpest. The same assumption is made for the  $T_{c3} = 44$  K phase. Based on this assumption, two repeatedly conducted experiments on different samples give  $x = 0.18$  for the  $T_{c2} = 36$  K phase and  $x = 0.35$  for the  $T_{c3} = 44$  K phase by integrating the leakage current. The Li content in the SC phase with  $T_{c3} = 44$  K,  $\text{Li}_{0.69(1)}\text{Fe}_2\text{Se}_2$ , is consistent with that of  $\text{Li}_{0.6(1)}(\text{ND}_2)_{0.2(1)}(\text{ND}_3)_{0.8(1)}\text{Fe}_2\text{Se}_2$  [35].

The successful realization of *in situ* tuning three SC phases in one device provides an ideal platform to investigate the evolution of their physical properties with doping. In the Supplemental Material, we present a systematic study of the anisotropic  $H_{c2}$  of  $\text{Li}_x\text{FeSe}$  [36]. The  $H_{c2}$  of  $\text{Li}_x\text{FeSe}$  shows a pronounced anisotropy upon increasing the Li content, which is distinct from the reported isotropic  $H_{c2}$  in FeAs-based superconductors [39] and the weak anisotropy of  $H_{c2}$  in  $\text{K}_x\text{Fe}_{2-y}\text{Se}_2$  [40], and even larger than those in  $(\text{Li}_{0.8}\text{Fe}_{0.2})\text{OHFeSe}$  and  $\text{Li}_x(\text{NH}_3)_y\text{Fe}_2\text{Se}_2$  [41,42]. By using the DFT calculation, we show that the combined

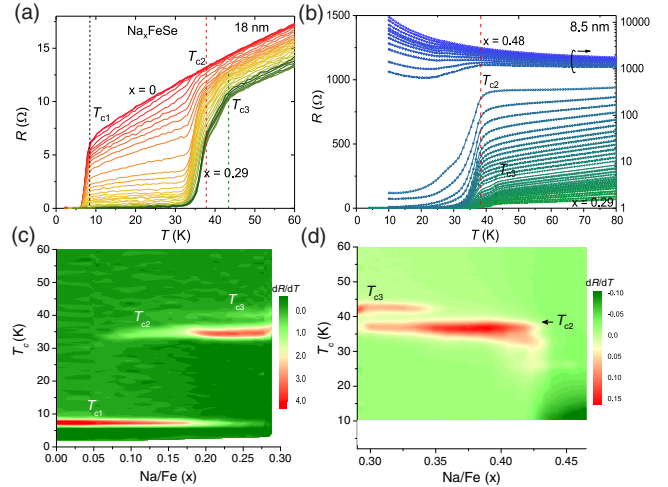


FIG. 3. (a) and (b) Resistance of Na-intercalated FeSe flakes as a function of temperature, similar to those of Fig. 2. The sample thicknesses are (a) 18 nm and (b) 8.5 nm. Vertical broken lines highlight transition temperatures where the  $T_c$ 's of different curves coincide.  $T_{c2}$  is observed throughout the entire doping region before the sample goes into the insulating phase. (c) and (d) Color contour plots of the derivatives of the  $R - T$  curves in (a) and rescaled in (b).

effects of Lifshitz transition, bandwidth narrowing and Se-Se interlayer coupling may be the driving force.

To examine whether the discrete SC phases are universal in other metal-intercalated FeSe, we carry out the experiment on a Na-based ionic substrate. As shown in Fig. 3, analogous with  $\text{Li}_x\text{FeSe}$ , there is a series of discrete SC transitions in  $\text{Na}_x\text{FeSe}$  at  $T_{c1} = 8$  K,  $T_{c2} = 37$  K, and  $T_{c3} = 43$  K. The observed 37 and 43 K SC phases in  $\text{Na}_x\text{FeSe}$  are consistent with the previously reported two SC phases with  $T_c \sim 37$  and 42 K in ammonia-free and ammonia-rich  $\text{Na}_x(\text{NH}_3)_y\text{FeSe}$  [43], and  $T_c \sim 32$  and 45 K in  $(\text{NH}_3)_y\text{Na}_x\text{FeSe}$  by changing the nominal Na content [44]. Our results suggest that the Na content determines the  $T_c$  of  $\text{Na}_x\text{FeSe}$ , in agreement with Ref. [44]. This is in line with a recent theoretical calculation which shows that the  $T_c$  is mainly determined by carrier concentration in intercalated FeSe [45]. The observation of discrete superconducting phases in both  $\text{Li}_x\text{FeSe}$  and  $\text{Na}_x\text{FeSe}$  demonstrates that the absence of a continuous superconducting dome is intrinsic and universal in metal-intercalated FeSe.

To check the robustness of this phase discreteness, we introduce disorder at the Se and Fe sites in FeSe. The substitution of S for Se has been proven to induce both disorder and chemical pressure, while the substitution of Cu for Fe introduces a negligible amount of electron doping, and most prominently, disorder [46,47]. The  $T_c$ 's of  $\text{FeSe}_{0.8}\text{S}_{0.2}$  and  $\text{Fe}_{0.98}\text{Cu}_{0.02}\text{Se}$  used here are 5 K and  $< 2$  K, respectively (see Fig. S3 in the Supplemental Material [27]), which agree well with the literature and confirm that Cu substitution has a much stronger effect

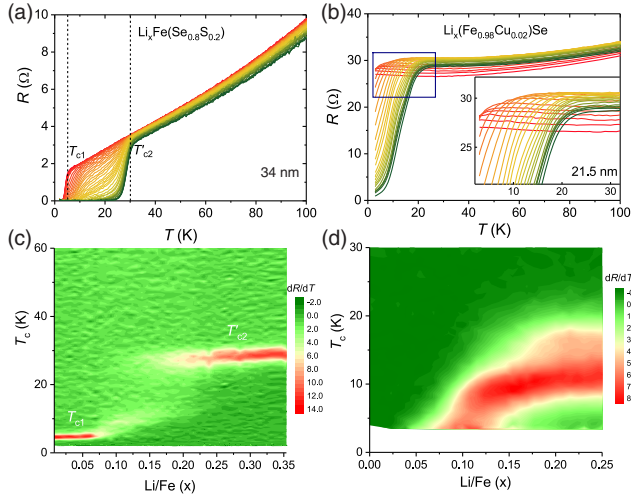


FIG. 4. (a) and (b) The gating dependence of  $R - T$  curves for  $\text{FeSe}_{0.8}\text{S}_{0.2}$  (34 nm thick) and  $\text{Fe}_{0.98}\text{Cu}_{0.02}\text{Se}$  (21.5 nm thick). (c) and (d) Their respective  $dR/dT$  color contour plots. Note that the  $T'_{c2}$  of  $\text{Li}_x\text{Fe}(\text{Se}_{0.8}\text{S}_{0.2})$  may not necessarily correspond to  $T_{c2}$  in  $\text{Li}_x\text{FeSe}$ . The inset in (b) expands the SC onset region.

on the superconductivity of FeSe. Figure 4(a) shows the resistance as a function of temperature during the gating process for  $\text{FeSe}_{0.8}\text{S}_{0.2}$ . The first SC transition at  $T_{c1}$  becomes broader, and the onset  $T_c$  gradually increases from 5 K to about 11 K, and then abruptly increases to  $T_{c2} = 30$  K. No higher  $T_c$  phase is observed upon further gating. The  $T_{c3}$  phase is completely destroyed by the substitution of S for Se. These two discrete SC phases are clearly visible in the derivative in Fig. 4(c), which rules out the possible origin of nematic inducing discrete SC phases, as the nematic order in FeSe is completely suppressed by 20% S doping. As shown in Fig. 4(b), starting from a non-SC ( $T_c < 2$  K)  $\text{Fe}_{0.98}\text{Cu}_{0.02}\text{Se}$  thin flake, the superconductivity emerges upon gating, and the onset  $T_c$ , shown in the inset, gradually increases to 23 K. The quasicontinuous evolution of  $T_c$  in  $\text{Li}_x(\text{Fe}_{0.98}\text{Cu}_{0.02})\text{Se}$  can be seen more clearly in Fig. 4(d), although two vague kinks are still visible at about 10 and 16 K. Further increasing the Cu content to 4% leads to a smooth increment of  $T_c$  without any kink, as shown in Fig. S4 in the Supplemental Material [27]. This demonstrates that the substitution of Cu for Fe not only suppresses superconductivity in FeSe, but also leads to a continuous change of  $T_c$  in  $\text{Li}_x\text{FeSe}$ , washing out the steps between the SC phases.

It is now possible to discuss the phase diagram of FeSe-derived superconductors in detail. The Fermi surface (FS) of bulk FeSe ( $T_c = 8$  K) consists of both electron and hole pockets [48]. However, in FeSe-derived superconductors with a higher  $T_c$ , such as  $\text{K}_x\text{Fe}_{2-y}\text{Se}_2$ ,  $(\text{Li}_{0.8}\text{Fe}_{0.2})\text{OHFeSe}$ , and monolayer FeSe/STO, only electron pockets at the Brillouin zone corner have been observed [15,16,49,50]. A clear evolution of FS topology can be seen in surface K-doped FeSe films, where the hole pocket at the Brillouin

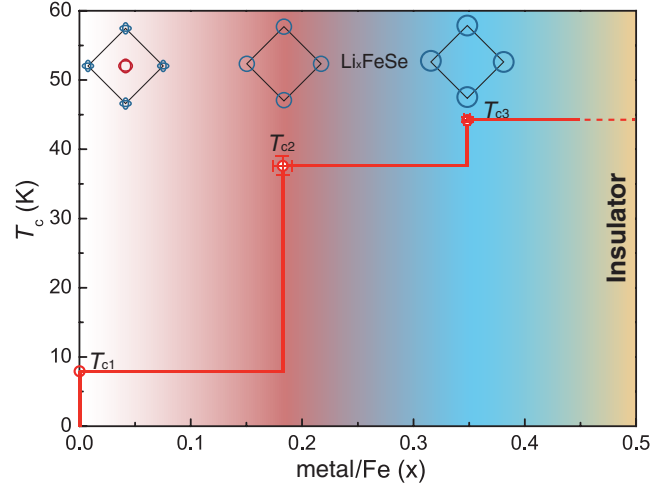


FIG. 5. Phase diagram of FeSe-derived superconductors. The red lines denote the discrete SC phases of metal-intercalated FeSe superconductors, as represented by  $\text{Li}_x\text{FeSe}$ . The different Fermi surface topologies of pristine and doped FeSe are superimposed. The yellow area on the right represents the insulating phase in the heavily overdoped region.

center shrinks to zero upon increasing the potassium dosage, leaving the Fermi surface with only electron pockets at the  $M$  point [13]. This Lifshitz transition of the FS topology is sketched in Fig. 5. In the recent electrostatic gating study on high-quality FeSe thin flakes, a steep  $T_c$  increase was observed around the Lifshitz transition [21]. Above this transition, the increase of  $T_c$  becomes more gradual and appears dome shaped [21], in agreement with the absence of a second Lifshitz transition and an enlarged electron Fermi surface at the  $M$  point upon further electron doping, as illustrated in Fig. 5. The sudden growth of  $T_c$  from 8 K to above 30 K could be caused either by a Lifshitz transition (i.e., a sudden change in the Fermi surface topology) or by an abrupt change in the pairing strength. Some mechanisms such as inter-pocket pairing between electron pockets [51] and orbital-selective pairing [52] were suggested for the higher- $T_c$  phase.

Aside from surface doping, extensive studies focusing on the metal-intercalated FeSe superconductors failed to depict phase diagram with carrier doping. Based on our present study, the phase diagram of metal-intercalated FeSe, represented by  $\text{Li}_x\text{FeSe}$ , is plotted as the red lines in Fig. 5. This solves the puzzle of the observation of only certain  $T_c$ 's for all the previously reported metal-intercalated FeSe superconductors [10,18,19], as well as a series of metal-intercalated superconductors containing organic molecules,  $\text{A}_x\text{R}_y\text{Fe}_2\text{Se}_2$  ( $A$  = intercalation metals,  $R$  = organic molecule) even when intentionally varying the initial doping content [53]. Furthermore, our Fe- and Se-substitution experiments demonstrate that this intrinsic discreteness is easily destroyed by disorder on the Fe site.

This behavior is similarly observed for cuprates, where a few-percent disorder on the copper site has a huge effect on the physical properties, including the superconductivity.

Our experiments constitute direct evidence of a discrete superconducting phase diagram as a function of carrier concentration in FeSe derivatives, which is clearly distinct from all other observations on unconventional superconductors [3]. In the electrostatic gating process using ionic liquids, the large cations from the electrolyte accumulate at the surface of FeSe, only doping electrons into the subsurface of FeSe [21]. Dosing potassium on the surface of FeSe thin film dopes electrons into the surface layer of FeSe too [54–56]. All these surface methods are different from the intercalation of Li and Na into the system driven by electric field, which induces carriers into the bulk of the system continuously. In the discrete SC phase diagram we report in Fig. 5, the transition between the different SC phases should be a first-order phase transition, which is very sensitive to disorder, possibly turning into a second-order transition. This may explain why the substitution of Cu for Fe not only suppresses superconductivity, but also leads to a continuous phase diagram. These results offer an insight into the mechanism of superconductivity in FeSe-derived superconductors.

We thank D. L. Feng, Y. Chen, J. P. Hu, N. Z. Wang, Y. Xu, and D. C. Peets for helpful discussions. This work was supported by the Ministry of Science and Technology of China (Grants No. 2016YFA0300503, No. 2015CB921401, and No. 2017YFA0303001), the Natural Science Foundation of China (Grant No. 11421404), the NSAF (Grant No. U1630248), the Key Research Program of Frontier Sciences CAS (Grant No. QYZDY-SSW-SLH021), and the China Postdoctoral Science Foundation (Grant No. 2016T90332).

T. P. Ying and M. X. Wang contributed equally to this work.

\*chenhx@ustc.edu.cn

†shiyang\_li@fudan.edu.cn

- [1] Y. Kamihara, T. Watanabe, M. Hirano, and H. Hosono, Iron-based layered superconductor  $\text{La}[\text{O}_{1-x}\text{F}_x]\text{FeAs}$  ( $x = 0.05\text{--}0.12$ ) with  $T_c = 26$  K, *J. Am. Chem. Soc.* **130**, 3296 (2008).
- [2] X. H. Chen, T. Wu, G. Wu, R. H. Liu, H. Chen, and D. F. Fang, Superconductivity at 43 K in  $\text{SmFeAsO}_{1-x}\text{F}_x$ , *Nature (London)* **453**, 761 (2008).
- [3] G. R. Stewart, Superconductivity in iron compounds, *Rev. Mod. Phys.* **83**, 1589 (2011).
- [4] S. Fujitsu, S. Matsuishi, and H. Hosono, Iron based superconductors processing and properties, *Int. Mater. Rev.* **57**, 311 (2012).
- [5] E. Dagotto, The unexpected properties of alkali metal iron selenide superconductors, *Rev. Mod. Phys.* **85**, 849 (2013).
- [6] X. H. Chen, P. C. Dai, D. L. Feng, T. Xiang, and F.-C. Zhang, Iron-based high transition temperature superconductors, *National political science review* **1**, 371 (2014).
- [7] M. R. Norman, The challenge of unconventional superconductivity, *Science* **332**, 196 (2011).
- [8] F.-C. Hsu, J.-Y. Luo, K.-W. Yeh, T.-K. Chen, T.-W. Huang, P. M. Wu, Y.-C. Lee, Y.-L. Huang, Y.-Y. Chu, D.-C. Yan, and M.-K. Wu, Superconductivity in the PbO-type structure  $\alpha\text{-FeSe}$ , *Proc. Natl. Acad. Sci. U.S.A.* **105**, 14262 (2008).
- [9] S. Medvedev, T. M. McQueen, I. A. Troyan, T. Palasyuk, M. I. Erements, R. J. Cava, S. Naghavi, F. Casper, V. Ksenofontov, G. Wortmann, and C. Felser, Electronic and magnetic phase diagram of  $\beta\text{-Fe}_{1.01}\text{Se}$  with superconductivity at 36.7 K under pressure, *Nat. Mater.* **8**, 630 (2009).
- [10] J. G. Guo, S. F. Jin, G. Wang, S. C. Wang, K. X. Zhu, T. T. Zhou, M. He, and X. L. Chen, Superconductivity in the iron selenide  $\text{K}_x\text{Fe}_2\text{Se}_2$  ( $0 \leq x \leq 1.0$ ), *Phys. Rev. B* **82**, 180520 (2010).
- [11] T. P. Ying, X. L. Chen, G. Wang, S. F. Jin, T. T. Zhou, X. F. Lai, H. Zhang, and W. Y. Wang, Observation of superconductivity at 30 ~ 46 K in  $\text{A}_x\text{Fe}_2\text{Se}_2$  ( $\text{A} = \text{Li, Na, Ba, Sr, Ca, Yb, and Eu}$ ), *Sci. Rep.* **2**, 426 (2012).
- [12] X. F. Lu, N. Z. Wang, H. Wu, Y. P. Wu, D. Zhao, X. Z. Zeng, X. G. Luo, T. Wu, W. Bao, G. H. Zhang, F. Q. Huang, Q. Z. Huang, and X. H. Chen, Coexistence of superconductivity and antiferromagnetism in  $(\text{Li}_{0.8}\text{Fe}_{0.2})\text{OHFeSe}$ , *Nat. Mater.* **14**, 325 (2015).
- [13] Y. Miyata, K. Nakayama, K. Sugawara, T. Sato, and T. Takahashi, High-temperature superconductivity in potassium-coated multilayer FeSe thin films, *Nat. Mater.* **14**, 775 (2015).
- [14] Q.-Y. Wan, Z. Li, W.-H. Zhang, Z.-C. Zhang, J.-S. Zhang, W. Li, H. Ding, Y.-B. Ou, P. Deng, K. Chang, J. Wen, C.-L. Song, K. He, J.-F. Jia, S.-H. Ji, Y.-Y. Wang, L.-L. Wang, X. Chen, X.-C. Ma, and Q.-K. Xue, Interface-induced high-temperature superconductivity in single unit-cell FeSe films on  $\text{SrTiO}_3$ , *Chin. Phys. Lett.* **29**, 037402 (2012).
- [15] S. Tan, Y. Zhang, M. Xia, Z. Ye, F. Chen, X. Xie, R. Peng, D. Xu, Q. Fan, H. Xu, J. Jiang, T. Zhang, X. C. Lai, T. Xiang, J. P. Hu, B. P. Xie, and D. L. Feng, Interface-induced superconductivity and strain-dependent spin density waves in FeSe/ $\text{SrTiO}_3$  thin films, *Nat. Mater.* **12**, 634 (2013).
- [16] S. He *et al.*, Phase diagram and electronic indication of high-temperature superconductivity at 65 K in single-layer FeSe films, *Nat. Mater.* **12**, 605 (2013).
- [17] J. J. Lee, F. T. Schmitt, R. G. Moore, S. Johnston, Y.-T. Cui, W. Li, M. Yi, Z. K. Liu, M. Hashimoto, Y. Zhang, D. H. Lu, T. P. Devereaux, D.-H. Lee, and Z.-X. Shen, Interfacial mode coupling as the origin of the enhancement of  $T_c$  in FeSe films on  $\text{SrTiO}_3$ , *Nature (London)* **515**, 245 (2014).
- [18] S. J. Shen, T. P. Ying, G. Wang, S. F. Jin, H. Zhang, Z. P. Lin, and X. L. Chen, Electrochemical synthesis of alkali-intercalated iron selenide superconductors, *Chin. Phys. B* **24**, 117406 (2015).
- [19] Y. Takahei, K. Tomita, Y. Itoh, K. Ashida, J.-H. Li, N. Nishimoto, T. Kimura, K. Kudo, M. Nohara, Y. Kubozono, and T. Kambe, A new way to synthesize superconducting metal-intercalated  $\text{C}_{60}$  and FeSe, *Sci. Rep.* **6**, 18931 (2016).
- [20] K. Ueno, S. Nakamura, H. Shimotani, A. Ohtomo, N. Kimura, T. Nojima, H. Aoki, Y. Iwasa, and M. Kawasaki,

- Electric-field-induced superconductivity in an insulator, *Nat. Mater.* **7**, 855 (2008).
- [21] B. Lei, J. H. Cui, Z. J. Xiang, C. Shang, N. Z. Wang, G. J. Ye, X. G. Luo, T. Wu, Z. Sun, and X. H. Chen, Evolution of High-Temperature Superconductivity from a Low- $T_c$  Phase Tuned by Carrier Concentration in FeSe Thin Flakes, *Phys. Rev. Lett.* **116**, 077002 (2016).
- [22] J. Shiogai, Y. Ito, T. Mitsuhashi, T. Nojima, and A. Tsukazaki, Electric-field-induced superconductivity in electrochemically etched ultrathin FeSe films on SrTiO<sub>3</sub> and MgO, *Nat. Phys.* **12**, 42 (2016).
- [23] K. Hanzawa, H. Sato, H. Hiramatsu, T. Kamiya, and H. Hosono, Electric field-induced superconducting transition of insulating FeSe thin film at 35 K, *Proc. Natl. Acad. Sci. U.S.A.* **113**, 3986 (2016).
- [24] Y. Saito, Y. Kasahara, J. Ye, Y. Iwasa, and T. Nojima, Metallic ground state in an ion-gated two-dimensional superconductor, *Science* **350**, 409 (2015).
- [25] B. Lei, N. Z. Wang, C. Shang, F. B. Meng, L. K. Ma, X. G. Luo, T. Wu, Z. Sun, Y. Wang, Z. Jiang, B. H. Mao, Z. Liu, Y. J. Yu, Y. B. Zhang, and X. H. Chen, Tuning phase transitions in FeSe thin flakes by field-effect transistor with solid ion conductor as the gate dielectric, *Phys. Rev. B* **95**, 020503 (2017).
- [26] Z. Z. Zhang, Q. Q. Zhang, C. Ren, F. Luo, Q. Ma, Y.-S. Hu, Z. B. Zhou, H. Li, X. J. Huang, and L. Q. Chen, A ceramic/polymer composite solid electrolyte for sodium batteries, *J. Mater. Chem.* **4**, 15823 (2016).
- [27] See Supplemental Material at <http://link.aps.org/supplemental/10.1103/PhysRevLett.121.207003> for detailed methods, which includes Refs. [26,28–34].
- [28] D. Chareev, E. Osadchii, T. Kuzmicheva, J.-Y. Lin, S. Kuzmichev, O. Volkovad, and A. Vasiliev, Single crystal growth and characterization of tetragonal FeSe<sub>1-x</sub> superconductors, *CrystEngComm* **15**, 1989 (2013).
- [29] G. Kresse and J. Hafner, Ab initio molecular dynamics for liquid metals, *Phys. Rev. B* **47**, 558 (1993).
- [30] G. Kresse and J. Furthmüller, Efficiency of ab initio total energy calculations for metals and semiconductors using a plane-wave basis set, *Comput. Mater. Sci.* **6**, 15 (1996).
- [31] G. Kresse and J. Furthmüller, Efficient iterative schemes for ab initio total-energy calculations using a plane-wave basis set, *Phys. Rev. B* **54**, 11169 (1996).
- [32] J. P. Perdew, K. Burke, and M. Ernzerhof, Generalized Gradient Approximation Made Simple, *Phys. Rev. Lett.* **77**, 3865 (1996).
- [33] S. Grimme, Semiempirical GGA-type density functional constructed with a long-range dispersion correction, *J. Comput. Chem.* **27**, 1787 (2006).
- [34] H. J. Monkhorst and J. D. Pack, Special points for Brillouin-zone integrations, *Phys. Rev. B* **13**, 5188 (1976).
- [35] M. Burrard-Lucas, D. G. Free, S. J. Sedlmaier, J. D. Wright, S. J. Cassidy, Y. Hara, A. J. Corkett, T. Lancaster, P. J. Baker, S. J. Blundell, and S. J. Clarke, Enhancement of the superconducting transition temperature of FeSe by intercalation of a molecular spacer layer, *Nat. Mater.* **12**, 15 (2013).
- [36] See Supplemental Material at <http://link.aps.org/supplemental/10.1103/PhysRevLett.121.207003> for anisotropic  $H_{c2}$  and DFT calculation of Li<sub>x</sub>FeSe, which includes Refs. [15,37–42].
- [37] J. L. Her, Y. Kohama, Y. H. Matsuda, K. Kindo, W.-H. Yang, D. A. Chareev, E. S. Mitrofanova, O. S. Volkova, and A. N. Vasiliev, Anisotropy in the upper critical field of FeSe and FeSe<sub>0.33</sub>Te<sub>0.67</sub> single crystals, *Supercond. Sci. Technol.* **28**, 045013 (2015).
- [38] J. Shiogai, S. Kimura, S. Awaji, T. Nojima, and A. Tsukazaki, Anisotropy of the upper critical field and its thickness dependence in superconducting FeSe electric-double-layer transistors, *Phys. Rev. B* **97**, 174520 (2018).
- [39] H. Q. Yuan, J. Singleton, F. F. Balakirev, S. A. Baily, G. F. Chen, J. L. Luo, and N. L. Wang, Nearly isotropic superconductivity in (Ba, K)Fe<sub>2</sub>As<sub>2</sub>, *Nature (London)* **457**, 565 (2009).
- [40] E. D. Mun, M. M. Altarawneh, C. H. Mielke, and V. S. Zapf, Anisotropic  $H_{c2}$  of K<sub>0.8</sub>Fe<sub>1.76</sub>Se<sub>2</sub> determined up to 60 T, *Phys. Rev. B* **83**, 100514(R) (2011).
- [41] C. L. Wang, X. L. Yi, Y. Qiu, Q. B. Tang, X. W. Zhang, Y. S. Luo, and B. H. Yu, Transport properties and anisotropy of superconducting (Li<sub>1-x</sub>Fe<sub>x</sub>)OHFeSe single crystals, *Supercond. Sci. Technol.* **29**, 055003 (2016).
- [42] S. S. Sun, S. H. Wang, R. Yu, and H. C. Lei, Extreme anisotropy and anomalous transport properties of heavily electron doped Li<sub>x</sub>(NH<sub>3</sub>)<sub>y</sub>Fe<sub>2</sub>Se<sub>2</sub> single crystals, *Phys. Rev. B* **96**, 064512 (2017).
- [43] J. G. Guo, H. C. Lei, F. Hayashi, and H. Hosono, Superconductivity and phase instability of NH<sub>3</sub>-free Na-intercalated FeSe<sub>1-z</sub>S<sub>z</sub>, *Nat. Commun.* **5**, 4756 (2014).
- [44] L. Zheng, X. Miao, Y. Sakai, M. Izumi, H. Goto, S. Nishiyama, E. Uesugi, Y. Kasahara, Y. Iwasa, and Y. Kubozono, Emergence of multiple superconducting phases in (NH<sub>3</sub>)<sub>y</sub>M<sub>x</sub>FeSe ( $M$ : Na and Li), *Sci. Rep.* **5**, 12774 (2015).
- [45] D. Guterding, H. O. Jeschke, P. Hirschfeld, and R. Valent, Unified picture of the doping dependence of superconducting transition temperatures in alkali metal/ammonia intercalated FeSe, *Phys. Rev. B* **91**, 041112 (2015).
- [46] A. Williams, T. McQueen, V. Ksenofontov, C. Felser, and R. Cava, The metal-insulator transition in Fe<sub>1.01-x</sub>Cu<sub>x</sub>Se, *J. Phys. Condens. Matter* **21**, 305701 (2009).
- [47] T.-W. Huang, T.-K. Chen, K.-W. Yeh, C.-T. Ke, C. L. Chen, Y.-L. Huang, F.-C. Hsu, M.-K. Wu, P. M. Wu, M. Avdeev, and A. J. Studer, Doping-driven structural phase transition and loss of superconductivity in M<sub>x</sub>Fe<sub>1-x</sub>Se ( $M$  = Mn, Cu), *Phys. Rev. B* **82**, 104502 (2010).
- [48] A. Subedi, L. Zhang, D. J. Singh, and M.-H. Du, Density functional study of FeS, FeSe, and FeTe: Electronic structure, magnetism, phonons, and superconductivity, *Phys. Rev. B* **78**, 134514 (2008).
- [49] T. Qian, X.-P. Wang, W.-C. Jin, P. Zhang, P. Richard, G. Xu, X. Dai, Z. Fang, J.-G. Guo, X.-L. Chen, and H. Ding, Absence of a Holelike Fermi Surface for the Iron-Based K<sub>0.8</sub>Fe<sub>1.7</sub>Se<sub>2</sub> Superconductor Revealed by Angle-Resolved Photoemission Spectroscopy, *Phys. Rev. Lett.* **106**, 187001 (2011).
- [50] X. H. Niu, R. Peng, H. C. Xu, Y. J. Yan, J. Jiang, D. F. Xu, T. L. Yu, Q. Song, Z. C. Huang, Y. X. Wang, B. P. Xie, X. F. Lu, N. Z. Wang, X. H. Chen, Z. Sun, and D. L. Feng, Surface electronic structure and isotropic superconducting gap in (Li<sub>0.8</sub>Fe<sub>0.2</sub>)OHFeSe, *Phys. Rev. B* **92**, 060504 (2015).

- [51] M. Khodas and A. V. Chubukov, Interpocket Pairing and Gap Symmetry in Fe-Based Superconductors with Only Electron Pockets, *Phys. Rev. Lett.* **108**, 247003 (2012).
- [52] E. M. Nica, R. Yu, and Q. Si, Orbital-selective pairing and superconductivity in iron selenides, *npj Quantum Mater.* **2**, 24 (2017).
- [53] T. P. Ying, X. L. Chen, G. Wang, S. F. Jin, X. F. Lai, T. T. Zhou, H. Zhang, S. J. Shen, and W. Y. Wang, Superconducting phases in potassium-intercalated iron selenides, *J. Am. Chem. Soc.* **135**, 2951 (2013).
- [54] C.-L. Song, H.-M. Zhang, Y. Zhong, X.-P. Hu, S.-H. Ji, L. L. Wang, K. He, X.-C. Ma, and Q.-K. Xue, Observation of Double-Dome Superconductivity in Potassium-Doped FeSe Thin Films, *Phys. Rev. Lett.* **116**, 157001 (2016).
- [55] C. H. P. Wen, H. C. Xu, C. Chen, Z. C. Huang, X. Lou, Y. J. Pu, Q. Song, B. P. Xie, M. Abdel-Hafiez, D. A. Chareev, A. N. Vasiliev, R. Peng, and D. L. Feng, Anomalous correlation effects and unique phase diagram of electron-doped FeSe revealed by photoemission spectroscopy, *Nat. Commun.* **7**, 10840 (2016).
- [56] W. H. Zhang, X. Liu, C. H. P. Wen, R. Peng, S. Y. Tan, B. P. Xie, T. Zhang, and D. L. Feng, Effects of surface electron doping and substrate on the superconductivity of epitaxial FeSe films, *Nano Lett.* **16**, 1969 (2016).